Component Dynamics in Miscible Blends: Equally and Unequally Entangled Polyisoprene/Polyvinylethylene

B. H. Arendt, R. Krishnamoorti,† and J. A. Kornfield*

Division of Chemistry and Chemical Engineering, California Institute of Technology, Pasadena, California 91125, and Department of Chemical Engineering, University of Houston, Houston, Texas 77204

S. D. Smith

Procter and Gamble Company, Cincinnati, Ohio 45239

Received June 21, 1996; Revised Manuscript Received December 3, 1996[⊗]

ABSTRACT: Miscible blends of 1,4-polyisoprene (PIP) and polyvinylethylene (PVE) are studied using rheo-optical methods to extract the dynamics of each component in the blend. Since orientational coupling contributes to the birefringence, but not the stress, simultaneous analysis of these observables for bidisperse blends is used to determine the coupling coefficient, ϵ. No systematic dependence of ϵ on composition or temperature was detected. The dynamics of the blend components extracted using the mean value of ϵ are in good agreement with those observed previously for equally entangled blends: blending causes only small changes in the component entanglement molecular weights but dramatically alters the species' friction coefficients, with the dynamics of the high T_g species (PVE) being more sensitive to both temperature and composition.

1. Introduction

Polymer blends are usually phase-separated systems consisting of at least two chemically distinct homopolymers, and often include a compatibilizer, such as a block or graft copolymer. To successfully predict the processing behavior of blends and formulate useful "blending rules" it is necessary to understand how the viscoelastic properties of each phase vary with composition and temperature. On a molecular level, the central issue is how the dynamics of each component are changed by blending. Approaches to obtain this information include infrared dichroism[1,2] flow birefringence,[3−7] and NMR relaxation times,[8] line width,[9] and multidimensional spectroscopy.[10−12] Here we adopt a rheo-optical approach that provides direct information on the conformational relaxation of each species and their relationship to the dynamic mechanical properties of a miscible blend.[4]

Single-phase blends provide useful model systems for a given phase in an immiscible blend. The choice of model system is further guided by the fact that most blends are phase separated, motivating study of species that do not attract each other. We examine blends of 1,4-polyisoprene (PIP) and polyvinylethlyene (PVE) since they are miscible, yet have negligible attractive interactions ($\chi \approx 0$).[13−17] PIP/PVE are also interesting because the components have widely disparate glass transition temperatures and mobilities,[4,7,9,18] as is usually the case for commercial blends.

Our previous work focused on effects unique to blends of chemically distinct polymers rather than features that exist even in bidisperse blends of a single species, such as constraint release.[19−21] Therefore, we studied PIP/PVE blends in which the two components were approximately equally entangled.[4] By avoiding effects of polydispersity on the shape of the component relaxation spectra, we tested the concept that local variations in composition lead to failure of time−temperature superposition. The results showed that thermorheological complexity was instead associated with distinct temperature dependencies of the dynamics of each component.[4,22] The temperature and composition dependence of the component monomeric friction coefficients ($\zeta_{o,i}$) are different, with the dynamics of the high T_g species (PVE) being more sensitive to temperature and composition.

Precise analysis of the rheo-optical results to determine the contribution of each species to the blend viscoelasticity includes the effect of orientational coupling. The present measurements on unequally entangled PIP/PVE blends establish the value of the coupling coefficients $\epsilon_{PIP,PVE}$ and $\epsilon_{PVE,PIP}$.[7,18] The results show that $\epsilon_{PIP,PVE} \approx \epsilon_{PVE,PIP}$. Therefore, we proceed to use an average value ϵ for all four ϵ_{ij}. Previous results on equally entangled blends and the present results for bidisperse blends are analyzed to determine the entanglement molecular weights and friction coefficients of each species as functions of ϕ and T. The results for several combinations of molecular weight are in good agreement.

The next section describes the properties of the PIP/PVE model system and rheo-optical technique, followed by the results of dynamic stress and birefringence measurements. The dependence of ϵ on temperature, composition, and species is then examined and found to be weak. Using this result, the stress−optical data are analyzed to determine the component dynamics in the blends. The sensitivity of the determination of the component entanglement molecular weights, $M_{e,i}$, and monomeric friction coefficients, $\zeta_{o,i}$, to orientational coupling is described.

2. Experimental Section

2.1. Materials. Blends of 1,4-polyisoprene (PIP) and 1,2-polybutadiene (polyvinylethylene) (PVE) were prepared using polymers synthesized by conventional anionic polymerization techniques.[22,24,25] The glass transition temperatures of the pure components were determined as the mid-point of the calorimetric transition on a Perkin Elmer DSC-7, using ∼25

* Correspondence to: Professor Julia A. Kornfield, Chemical Engineering 210-41, California Institute of Technology, Pasadena, CA 91125.
† University of Houston.
⊗ Abstract published in *Advance ACS Abstracts,* February 1, 1997.

S0024-9297(96)00901-1 CCC: $14.00

Table 1. Characterization of Polyisoprene (PIP) and Polyvinylethylene (PVE) Homopolymers

sample	M_w[a] (kg/mol)	M_w/M_n[a]	ω''_{max} (rad/s) at 25 °C	T_g (°C)[b]
E-PIP	190	1.09	2.3	−65.8
E-PVE	80	1.09	0.04	−2.1
S-PIP	110	1.05	14.0	−64.9
L-PVE	290	1.11	.0005	−2.5
L-PIP	850	1.17	0.022	−64.0
S-PVE	80	1.09	0.04	−2.1

[a] In THF at 25 °C, using PIP standards. [b] From DSC heating at 10 °C/min.

Table 2. Stress−Optic Coefficients of Polyisoprene (PIP) and Polyvinylethylene (PVE) Homopolymers[a]

	$C \times 10^{10}$ (cm^2/dyne)	
T (°C)	PIP	PVE
−10	1.8_8	-0.3_5
5	1.7_7	-0.2_8
15	1.7_3	-0.2_5
25	1.6_8	-0.2_3
40	1.6_2	-0.1_7
60	1.5_5	-0.1_0
80	1.4_7	-0.04_8
110	1.3_8	$+0.01_6$
130	1.3_0	$+0.05_0$

[a] Average of values for each type of polymer. Variation of values between different samples of the same species fall within the uncertainty in the measurements.

mg samples and 10 °C/min heating rate. The glass transition temperatures, which are sensitive to microstucture, indicate that the PVE contains > 95% 1,2-polybutadiene units (Table 1). Room temperature ^{13}C NMR on 25% w/v $CDCl_3$ solutions of the pure components using a General Electric QE-300 spectrometer confirmed the PVE microstructures and showed the PIP microstructures contain >94% 1,4-units. Molecular weights were determined by GPC in THF at 25 °C, calibrated using PIP standards from Polymer Laboratories. All of the polymers are well entangled and have narrow molecular weight distributions. The component stress−optic coefficients are of opposite signs (Table 2).[4] The relative length of the polymers is indicated by a prefix, E, S, or L, denoting equally entangled, short or long components (Table 1).

2.2. Rheo-optical Method. Dynamic mechanical and birefringence measurements are made using the same rheo-optical instrument as in our previous studies.[4,26,27] The strain, shear stress, birefringence, and its orientation are simultaneously recorded. We present the results of birefringence measured in the plane given by the velocity (direction 1) and the velocity gradient (direction 2), obtained with the optical beam along the vorticity axis (direction 3).

The experimental observables include the shear stress, σ_{12}, and the corresponding component of the refractive index tensor, n_{12}. When a sample is subjected to small amplitude oscillatory shear, $\gamma(t) = \gamma_o \sin \omega t$, both σ_{12} and n_{12} show linear responses:

$$\sigma_{12} = \gamma_o[G'(\omega) \sin \omega t + G''(\omega) \cos \omega t] \quad (1)$$

$$n_{12} = \gamma_o[B'(\omega) \sin \omega t + B''(\omega) \cos \omega t] \quad (2)$$

where $G'(\omega)$ and $G''(\omega)$ are the storage and loss moduli and $B'(\omega)$ and $B''(\omega)$ are the components of the complex birefringence coefficient, $B^*(\omega)$.[26,27] Departures from the stress−optic rule are examined using the amplitude-based stress−optic ratio SOR and the phase difference between σ_{12} and n_{12}:

$$\text{SOR} \equiv |B^*|/|G^*| \quad (3)$$

and

$$\delta_B - \delta_G \equiv \tan^{-1}(B''/B') - \tan^{-1}(G''/G') \quad (4)$$

Table 3. Shift Factors, a_T, of Homopolymers and E-PIP/E-PVE Blends

T	homopolymers			blends (PIP/PVE w/w %)		
(°C)	$b_{T,PIP}$	PIP	PVE	75/25	50/50	25/75
−10	1.09	46	−	90	500	−
5	1.02	6.9	1900	11	23	70
15	−	−	−	−	−	7.5
25	1	1	1	1	1	1
40	0.97	0.35	0.055	0.32	0.24	0.14
60	0.92	0.118	0.00355	0.086	0.048	0.0175
80	0.89	0.051	0.000495	0.032	0.014	0.0038
110	0.87	0.020	0.000064	0.0106	0.00375	0.00073

Table 4. Shift Factors, a_T, of Homopolymers and S-PIP/L-PVE Blends

	homopolymers			blends (PIP/PVE w/w %)		
T (°C)	$b_{T,PIP}$	PIP	PVE	75/25	50/50	25/75
−10	1.08	42	−	100	−	−
5	1.03	6.5	−	11	15	−
15	1.02	2.42	18	3.2	3.5	4.5
25	1	1	1	1	1	1
40	0.98	0.35	0.055	0.28	0.17	0.14
60	0.95	0.12	0.003 6	0.065	0.027	0.015
80	0.92	0.048	0.000 52	0.02	0.007	0.003
110	−	−	0.000 07	−	0.001 8	0.000 6

Table 5. Shift Factors, a_T, of Homopolymers and L-PIP/S-PVE Blends

	homopolymers			blends (PIP/PVE w/w %)		
T (°C)	$b_{T,PIP}$	PIP	PVE	75/25	50/50	25/75
25	1	1	1	1	1	1
40	0.98	0.34	0.055	0.32	0.18	0.10
60	0.96	0.107	0.003 5	0.095	0.041	0.012 3
80	0.89	0.044	0.000 46	0.035	0.013	0.003 23
110	0.87	0.016 3	0.000 061	0.012 5	0.004	0.000 77
130	0.84	0.01	−	0.008 5	0.002 3	0.000 4

For homopolymer melts, the stress−optic rule holds (SOR = C_i, the stress−optic coefficient of homopolymer i, and $\delta_B - \delta_G \approx 0$).[28] For miscible blends, deviations from the stress−optic rule provide a convenient means to determine the relaxation dynamics of each species.[3,4] This approach is well suited to blends in which the species have very different stress−optic coefficients (e.g., systems with C_i's of opposite sign, including PIP/PVE, PS/PPO and PS/PVME).

Frequencies from 0.01 to 100 rad/s were employed, at temperatures ranging from 5 to 110 °C. At high frequencies and low temperatures, oscillatory strains of 1% or less were applied. With decreasing frequency and increasing temperature, when the force signal decreased to the limit of the transducer, the strain was increased. At the highest temperatures (80 and 110 °C) and the lowest frequencies, strains of 50−100% were used. In all cases, it was verified that the birefringence and viscoelastic response were in the linear regime. Experiments at the lowest and highest temperatures were performed under nitrogen atmosphere. To prevent sample degradation, in addition to using an inert atmosphere at elevated temperatures, the exposed surfaces of the samples were coated with 2,6-di-*tert*-butyl-4-methylphenol (BHT). Selected samples were examined by GPC after a full suite of experiments; no evidence of degradation was found.

3. Results

3.1. Homopolymer Characterization. The dynamic moduli of all the pure components have a single loss peak. The homopolymers obey time−temperature superposition as expected,[29] with horizontal shift factors, $a_{T,i}$ (Table 3−5), that agree well with the previously established WLF behavior.[22,24,25] For the PVE homopolymers no vertical shifting was required to obtain superposition. The PIP homopolymers required values of $b_{T,i}$ close to unity, in accord with the literature.[25] (The

magnitudes of the cross-over and plateau moduli are consistently 27% lower than literature values.[7,18,24,25,29] While we have been unable to account for this deviation, all our data are self-consistent; thus, it does not affect the trends in the results.)

By comparing the dynamic birefringence to the dynamic modulus it was confirmed that the stress−optic rule holds away from the dynamic glass transition for all pure components,[28,30] with the stress−optic coefficients given in Table 2. Notice that the values of C_{PVE} are an order of magnitude smaller than C_{PIP} and also of opposite sign (for T < 100 °C). Thus, while the two species contribute similarly to the bulk stress, their contributions to the birefringence are of opposite sign over most of the experimental temperature range, which allows us to detect their distinct contributions.

Interestingly, C_{PVE} varies unusually strongly with temperature, and even changes sign, over the temperature range covered by our experiments. This behavior is quite unlike the sign change associated with the dynamic glass transition in some polymers;[33] indeed, the authors are aware of no other polymer that exhibits such an anomalous temperature dependence of its stress−optic coefficient in the plateau and terminal regimes.

3.2. Characterization of Blends. Three series of blends, designated as E-PIP/E-PVE (equally entangled components), L-PIP/S-PVE (long PIP), and S-PIP/L-PVE (short PIP), were examined over a range of composition and temperature.

3.2.1. Dynamic Moduli. All three blend series exhibit complex thermorheological behavior, particularly for the L-PIP/S-PVE and S-PIP/L-PVE blends. The dynamic mechanical data obtained at different temperatures were shifted along the frequency axis only to superimpose the values at the lowest experimental frequencies ("mechanical shift factors" are given in Tables 3−5).

Like binary blends of a given polymer,[19,20,21,31] the low-frequency loss peak in the unequally entangled blends grows nonlinearly with the fraction of long chains (Figures 1−3). Unlike binary blends of the same polymer, increasing temperature shifts the relative frequency of the high-frequency loss peak compared to the low-frequency peak. Increasing the fraction of PIP chains shifts the positions of both loss peaks to higher reduced frequency (moving from Figure 2c to b to a and from Figure 3c to b to a). Furthermore, in both blend systems, the dynamics of PVE are much more sensitive to composition than those of PIP, in accord with previous results.[4,12,18,22]

3.2.2. Dynamic Birefringence. The stress−optic data are displayed using the same reduced frequency as the dynamic moduli (Figures 4−9). Three main features are evident in the frequency dependence of the SOR for all three blend systems (Figures 4, 6, and 8): a high-frequency plateau, a step at intermediate frequencies, and a low-frequency plateau. In the case of the E-PIP/E-PVE and L-PIP/S-PVE blends the low-frequency plateau is greater than the high-frequency plateau, due to the faster relaxation of the PVE which has a negative pure-component SOR. In contrast, the S-PIP/L-PVE blends have a low-frequency plateau that is smaller than the high-frequency plateau. The phase difference between the stress and the birefringence ($\delta_B - \delta_G$) (Figures 5, 7, and 9) shows significant deviations from zero, with the presence of dips (E-PIP/E-PVE and L-PIP/S-PVE) or humps (S-PIP/L-PVE) at frequencies near the steps in the corresponding SOR.

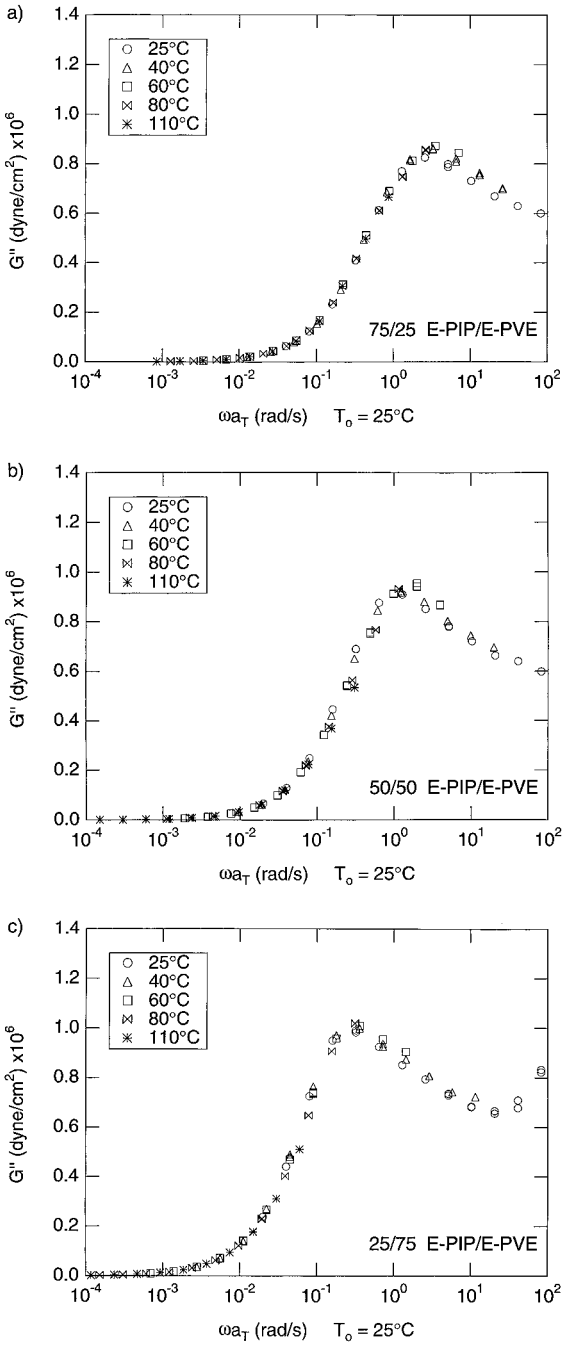

Figure 1. Loss moduli "master curves" for **(**a**)** 75/25 E-PIP/E-PVE, **(**b**)** 50/50 E-PIP/E-PVE, and **(**c**)** 25/75 E-PIP/E-PVE blends. The reference temperature is T_o = 25 °C. Note that time−temperature superposition appears to hold for all of the samples. Only a horizontal shift was used to superimpose the data in the terminal regime.

3.3. Blend Plateau Moduli and High-Frequency SOR. The magnitude of the blend plateau modulus, G_N^o, is estimated from the value of the storage modulus, $G'(\omega''_{min})$, where the loss modulus reaches a minimum above the higher frequency loss peak.[29] In this regime both species contribute to the blend plateau modulus. For all three blend systems the values follow an essentially linear weighting between the pure component values (Figure 10), as seen previously.[4]

The high-frequency plateau in the blend SOR also follows a linear weighting of the pure component C_i's (Figure 11). The linear behavior suggests that the homopolymer stress−optic coefficients do not change significantly upon blending in the PIP/PVE system and

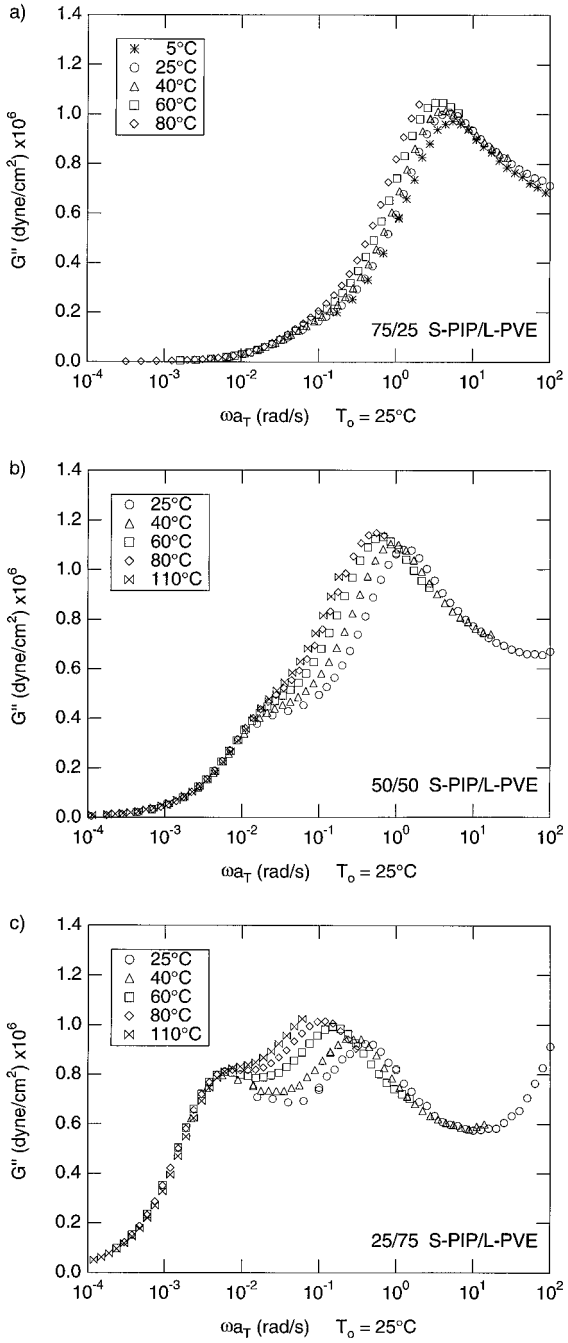

Figure 2. Loss moduli "master curves" for **(**a**)** 75/25 S-PIP/L-PVE, **(**b**)** 50/50 S-PIP/L-PVE, and **(**c**)** 25/75 S-PIP/L-PVE blends. The reference temperature is T_o = 25 °C. Note that time−temperature superposition does *not* hold for any of the samples. Only a horizontal shift was used to superimpose the data in the terminal regime.

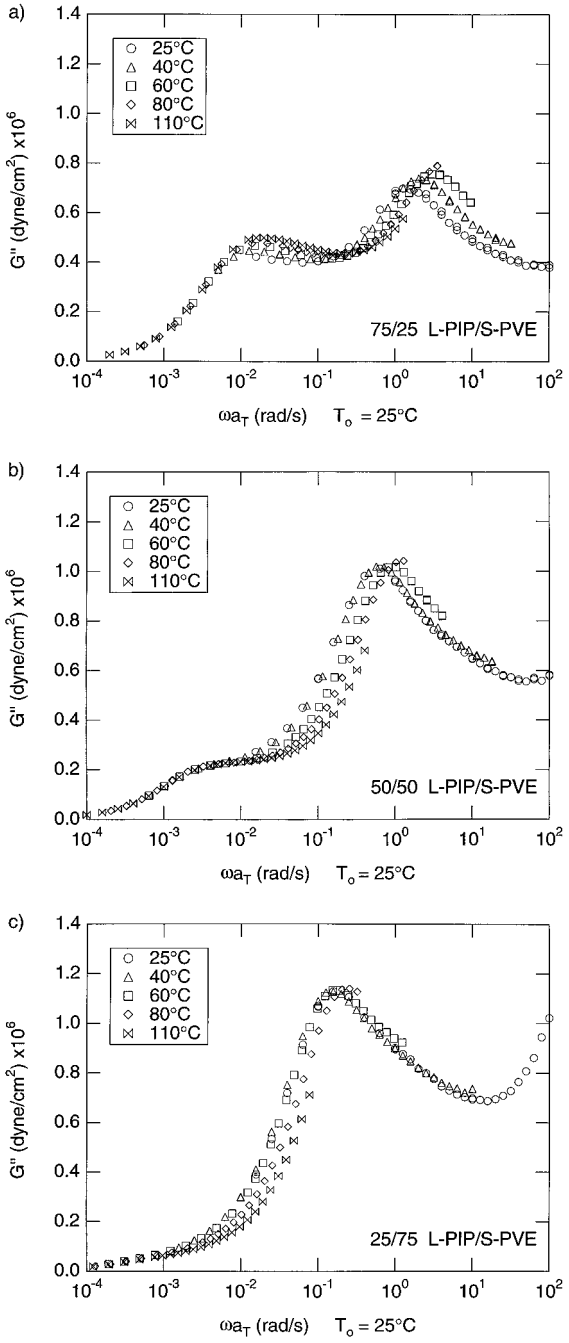

Figure 3. Loss moduli "master curves" for **(**a**)** 75/25 L-PIP/S-PVE, **(**b**)** 50/50 L-PIP/S-PVE, and **(**c**)** 25/75 L-PIP/S-PVE blends. The reference temperature is T_o = 25 °C. Note that time−temperature superposition does *not* hold for any of the samples. Only a horizontal shift was used to superimpose the data in the terminal regime.

supports the use of the pure-component stress−optic coefficients to interpret the stress−optic behavior of the blends.

4. Discussion

Unlike the E-PIP/E-PVE blends, where only a single loss peak is observed at all compositions, the unequally entangled blends display two loss peaks when the blends contain sufficient amounts of the long chains ($\phi_L \geq 0.5$), with the peak at lower frequency corresponding to this slower relaxing species. Comparing the position of the loss peaks in these blends with those of the homopolymers (Table 1) shows that the dynamics of PVE are greatly accelerated in the blends while those of PIP are only slightly retarded. For the S-PIP/L-PVE blends that have two loss peaks, the separation between the peaks diminishes with increasing temperature (Figure 2), while in the L-PIP/S-PVE blends the separation increases with increasing temperature (Figure 3). In both cases the relative shift indicates that the dynamics of PVE speed up more strongly with temperature than those of PIP, particularly in blends rich in PVE (Tables 3−5), in accord with previous studies.[4,12,18,22]

All three blend systems show high- and low-frequency plateaus in SOR and a step at intermediate frequencies (Figures 4, 6, and 8). As discussed in our earlier work,[4] the high-frequency plateau indicates a regime where

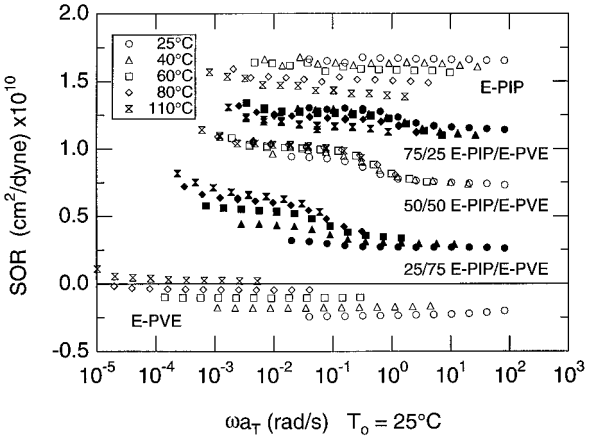

Figure 4. SOR of the E-PIP/E-PVE blends vs the same reduced frequencies as the dynamic moduli of the respective samples. Shown for comparison are the stress−optic coefficients of the pure components.

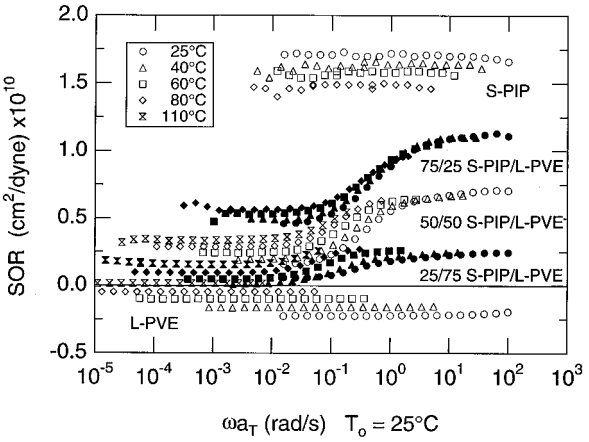

Figure 6. SOR of the S-PIP/L-PVE blends vs the same reduced frequencies as the dynamic moduli of the respective samples. Shown for comparison are the stress−optic coefficients of the pure components.

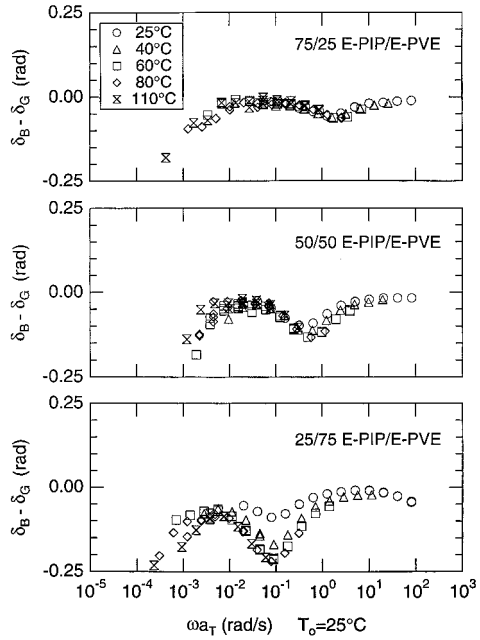

Figure 5. Phase difference between the dynamic birefringence and shear stress for the E-PIP/E-PVE blends.

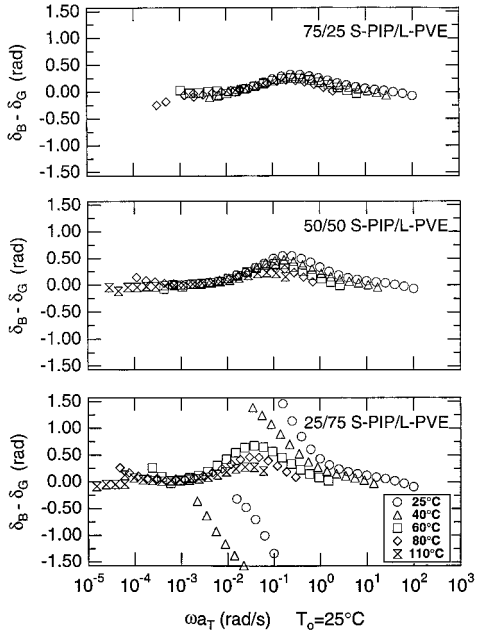

Figure 7. Phase difference between the dynamic birefringence and shear stress for the S-PIP/L-PVE blends.

both species contribute to the stress and birefringence, and SOR is simply a weighted average of the pure component C_i's. The step in the magnitude of SOR moves in the direction of the stress−optic coefficient of the slower relaxing species in the blend (upward step for L-PIP/S-PVE and downward step for S-PIP/L-PVE). Indeed, the step up in SOR of E-PIP/E-PVE with decreasing ω reveals that PVE relaxes first, although the two species nearly relax at the same rate.[4] The low-frequency plateau corresponds to frequencies where both species are in their terminal relaxation regime.

The effects of blend ratio and temperature on the inflection in SOR reflect their effects on the dynamics of the faster relaxing species. With increasing PIP content the frequency of the upturn or downturn in the SOR increases, particularly in blends in which PVE is the faster relaxing species. With increasing temperature the inflection in SOR shifts to higher ωa_T when PVE is the faster relaxing species (i.e., E-PIP/E-PVE and L-PIP/S-PVE) and to lower reduced frequencies for S-PIP/L-PVE. The effect of temperature is most dramatic for blends rich in PVE.

As discussed in our previous work,[4] a dip in $\delta_B - \delta_G$ is characteristic of blends in which PVE is faster relaxing, whereas a hump in $\delta_B - \delta_G$ is expected in blends with short PIP. Indeed, the S-PIP/L-PVE blends exhibit a hump rather than a dip (Figure 7). For $\phi_{PIP} = 0.25$, at the lowest temperatures $\delta_B - \delta_G$ passes through $+\pi/2$, represented by a drop to $-\pi/2$ when the range is restricted to $\pm\pi/2$. The phase difference exceeds $\pi/2$ where the values of B' are negative while those of B'' are positive, indicating that the contribution from PVE is becoming dominant as the frequency decreases. On the other hand, the E-PIP/E-PVE and L-PIP/S-PVE blends show a dip in $\delta_B - \delta_G$, indicating the PVE component relaxes first (Figures 5 and 9). In all three systems the position of the feature (dip or hump) tracks the inflection in SOR as a function of PIP content and temperature.

To be more quantitative, the stress−optic data are analyzed to determine the component moduli in the blends.

4.1. Determining the Component Moduli in the Blends. Analogous to the approach taken in describing

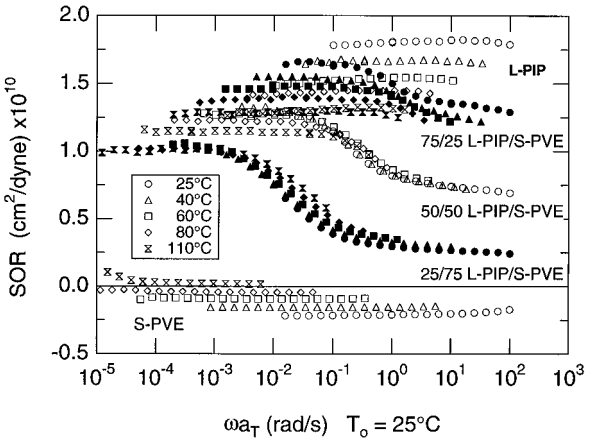

Figure 8. SOR of the L-PIP/S-PVE blends vs the same reduced frequencies as the dynamic moduli of the respective samples. Shown for comparison are the stress−optic coefficients of the pure components.

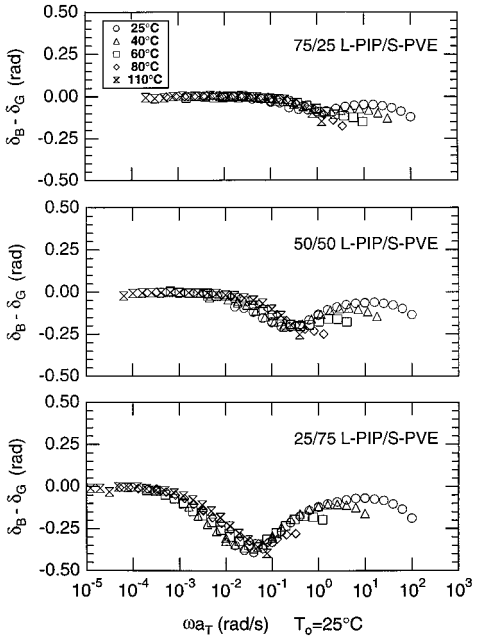

Figure 9. Phase difference between the dynamic birefringence and shear stress for the L-PIP/S-PVE blends.

binary blends of polymers of identical chemical structure,[19−21] the bulk stress in a miscible blend is the sum of the entropic stresses due to conformational distortion of each component in the blend. Thus, the corresponding dynamic moduli are given by

$$G^*_{\text{blend}}(\omega;\phi_A,T) = \phi_A G^*_A(\omega;\phi_A,T) + \phi_B G^*_B(\omega;\phi_A,T) \quad (5)$$

where $G^*_i(\omega;\ \phi_A,T)$ denotes the relaxation spectrum of species i when it is in a blend of composition ϕ_A (volume fraction of component A, with i = A or B). The relaxation dynamics of each species in the blend may be modified from those of the homopolymer (e.g., by constraint release). This is evident when the components have well-separated terminal relaxation times in the blend.[22] The experimental values of G^*_{blend} and B^*_{blend} provide two observables that can be used to determine $G^*_A(\omega;\ \phi_A,T)$ and $G^*_B(\omega;\ \phi_A,T)$. For this purpose we measure the *corresponding* components of the stress and refractive index tensors, σ_{12} and n_{12} (eqs 1 and 2). These two quantities are measured simultaneously on the same instrument and do not rely on constitutive

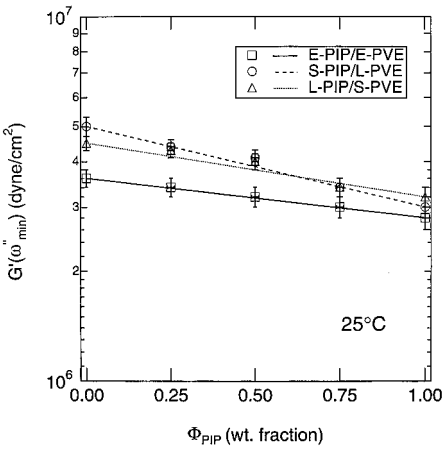

Figure 10. Plateau modulus for the blends and pure components versus weight percent PIP, at T = 25 °C. The lines represents the composition-weighted average of the homopolymer values.

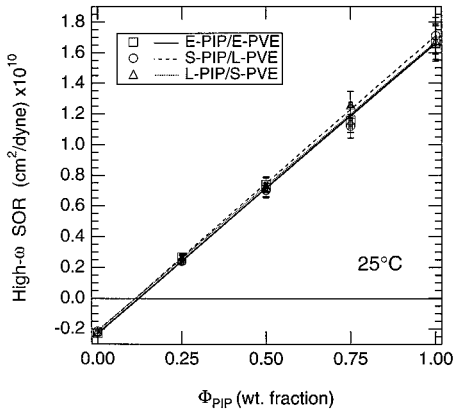

Figure 11. Magnitude of the high-frequency plateau in SOR (high-ω SOR) for all the blends versus weight percent PIP, at T = 25 °C. The solid line represents the composition-weighted average of the homopolymer stress−optic coefficients.

relations or extrapolation to relate the mechanical and optical measurements.[7]

The analysis used to determine G^*_A and G^*_B is influenced by orientational coupling, currently viewed as a packing effect[34] that couples the orientation of a given chain to the orientation of the surrounding matrix. When orientational coupling is present, each component contributes to the birefringence not only in proportion to its own dynamic modulus, but also in proportion to the local orientation imposed by both like and unlike neighboring bonds via orientational coupling. In this case, the birefringence of the blend is given by

$$B^*_{\text{blend}} = C_A[\phi_A G^*_A - \epsilon\phi_A\phi_B(G^*_B - G^*_A)] + C_B[\phi_B G^*_B - \epsilon\phi_A\phi_B(G^*_A - G^*_B)] \quad (6)$$

where ϵ denotes the average coupling coefficient, C_i is the stress−optic coefficient of pure component i and ϕ_i is the volume fraction of that component in the blend.[7,18,35] The possible values of ϵ lie between 0 (no coupling) and 1 (complete coupling). When $\epsilon = 0$, eq 6 reduces to the expression used in our previous work.[4] By using eqs 5 and 6, the underlying component moduli in the blend, $G^*_A(\omega;\phi_A,T)$ and $G^*_B(\omega;\phi_A,T)$, can be determined from the blend dynamic moduli and birefringence coefficients using established values of C_A, C_B, and ϵ.

In the above equation, ϵ denotes the average of four distinct coupling coefficients, $\epsilon_{\text{PIP,PIP}}$, $\epsilon_{\text{PVE,PVE}}$, $\epsilon_{\text{PIP,PVE}}$,

and $\epsilon_{PVE,PIP}$, which describe coupling between like species, PIP to PIP and PVE to PVE, and between unlike species, PIP to PVE and PVE to PIP, respectively. Without sufficient information to determine all four coupling coefficients, we test the hypothesis that an average value of ϵ will be a good approximation by examining two sets of blends, one where the short component is PIP and one where it is PVE.

Orientational coupling has the consequence that a chain that is conformationally relaxed on the scale of entanglement strands and hence bears no stress, remains anisotropic on the local bond level if it exists in an oriented matrix of unrelaxed chains.[35] Thus, orientational coupling is clearly manifested in the low frequency behavior of unequally entangled blends. The magnitude of the effect of orientational coupling on the low-frequency plateau in SOR depends on the relative magnitudes of the stress−optic coefficients of the fast- and slow-relaxing species. In blends where PVE is the slow-relaxing species, we would expect it to dominate the stress−optic response at the lowest frequencies. At these low frequencies, PIP will contribute to the birefringence only due to orientational coupling. Since orientation of PIP gives a much larger birefringence than a corresponding orientation of PVE, the orientation induced in PIP by coupling can significantly affect the low-frequency SOR plateau. Consequently, the coupling coefficient is fairly easily and accurately determined in S-PIP/L-PVE blends. On the other hand, in blends where PIP is the slower relaxing species, orientational coupling is manifested by the effect of PVE contributing to the low-frequency values of SOR. In this case, it is more difficult to ascertain the degree of coupling because the contribution of PVE is much smaller than the large, positive birefringence contribution of PIP. Hence the values of the coupling coefficients for the L-PIP/S-PVE blends have larger uncertainties (Figure 14).

The blend mechanical and optical data are analyzed iteratively to determine the component contributions, G^*_{PVE} and G^*_{PIP}, and ϵ. First, G^*_{PVE} and G^*_{PIP} are computed for a trial value of ϵ and the known values of C_A and C_B using eq 6. Then the resulting component dynamic moduli are examined to determine whether the trial value of ϵ was too large or too small. Values of ϵ that are too large lead to unphysical, negative values of the storage modulus for the faster relaxing component and terminal behavior that decays much steeper than $G'' \approx \omega$ and $G' \approx \omega^2$. Values of ϵ that are too small yield a storage modulus for the faster relaxing species that plateaus at low frequencies and does not achieve terminal behavior. The shape and terminal slopes of the calculated component moduli for the faster relaxing species are quite sensitive to the value of ϵ used. Consequently, when the relaxation times of the two species are well separated in the blend, it is possible to estimate the values of ϵ to within ± 0.02 (Figures 12 and 13).

The sensitivity with which we can determine ϵ does not include the effect of uncertainty in the pure component C_i's. Given a $\pm 10\%$ uncertainty in the pure component stress−optic coefficients, the values and uncertainty in the coupling coefficients are $\epsilon_{PIP,PVE} = 0.33 \pm 0.08$, 0.36 ± 0.07, and 0.36 ± 0.05 and $\epsilon_{PVE,PIP} = 0.23 \pm 0.14$, 0.28 ± 0.10, and 0.30 ± 0.10, for $\phi_{PIP} = 0.75$, 0.5, and 0.25, respectively (Figure 14). (Recall that $\epsilon_{i,j}$ refers to i coupling to a j matrix.) There appears to be no systematic dependence on temperature or composition in either system.[7,18,36] The absence of any

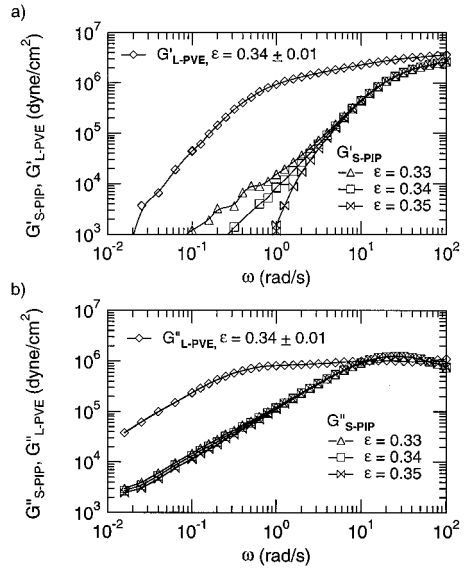

Figure 12. Figure detailing the determination of ϵ for a 50/50 blend of *S*-PIP/L-PVE at 60 °C, showing how it can be determined within ± 0.01 by observing the terminal behavior of the faster relaxing species in the blend. See the text for discussion.

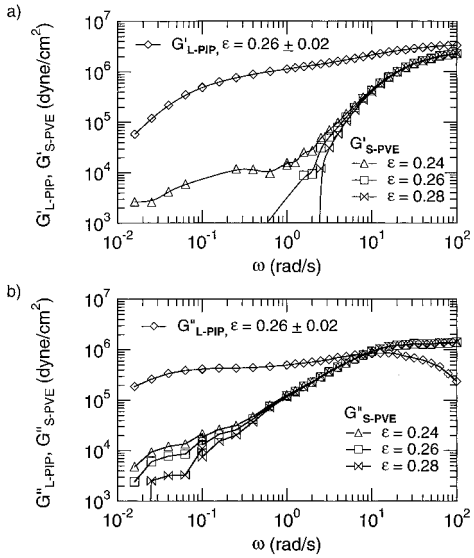

Figure 13. Figure detailing the determination of ϵ for a 50/50 blend of L-PIP/S-PVE at 60 °C, showing how it can be determined within ± 0.02 by observing the terminal behavior of the faster relaxing species in the blend. Notice the larger uncertainty in these blends. See the text for discussion.

temperature dependence, at least over the limited temperature range probed in these experiments, is in accord with proposed entropic origins for orientational coupling.[36]

The values of ϵ for both blend systems lie between 0.20 and 0.40 over the range of compositions and temperatures probed (Figure 14). These values fall within the range previously established for various systems.[7,18,36] Although the values of $\epsilon_{PIP,PVE}$ are somewhat higher than $\epsilon_{PVE,PIP}$, the difference between the two lies within the uncertainty in the measurements, suggesting that a single average value of ϵ is capable of describing the coupling in the PIP/PVE system.

We analyze the component moduli for blends by incorporating the effects of orientational coupling using the value $\epsilon \approx 0.35$, which accords with the observed values of ϵ to within experimental uncertainty. The

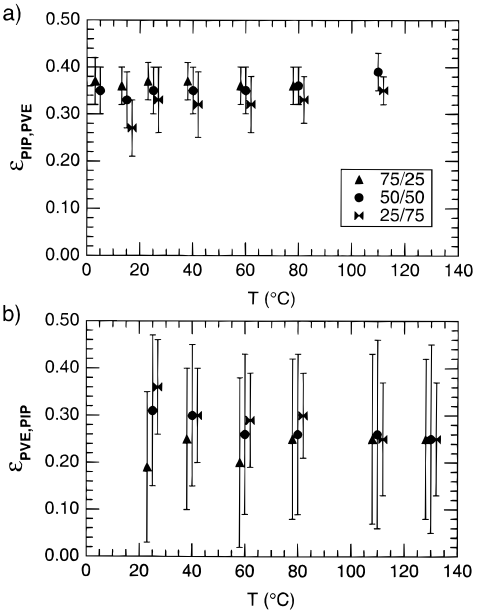

Figure 14. Values of the coupling coefficient determined for the (a) S-PIP/L-PVE and **(**b**)** L-PIP/S-PVE blends. Values for $\phi_{PIP} = 0.75$ and 0.25 are offset horizontally from those for $\phi_{PIP} = 0.5$ for clarity; the filled circles ($\phi_{PIP} = 0.5$) are unshifted. Error bars indicate the uncertainty in the values, including those when a ±10% uncertainty in the component stress−optic coefficients is assumed. See the text for discussion.

Table 6. Shift Factors, $a_{T,i}$, of Each Species in E-PIP/ E-PVE Blends

	blends (PIP/PVE w/w %)					
	75/25		50/50		25/75	
T (°C)	PIP	PVE	PIP	PVE	PIP	PVE
−10	90	160	290	800	−	−
5	11	15	18	30	49	80
15	−	−	−	−	6	7.9
25	1	1	1	1	1	1
40	0.32	0.33	0.25	0.2	0.18	0.131
60	0.088	0.089	0.051	0.039	0.028	0.015
80	0.033	0.03	0.016	0.009 4	0.007	0.002 9
110	0.011	0.01	0.004 4	0.002 1	0.001 5	0.000 5

Table 7. Shift Factors, $a_{T,i}$, of Each Species in S-PIP/ L-PVE Blends

	blends (PIP/PVE w/w %)					
	75/25		50/50		25/75	
T (°C)	PIP	PVE	PIP	PVE	PIP	PVE
−10	88	105	−	−	−	−
5	10	11	12.5	19	−	−
15	3.2	3.6	3.15	4.4	4.0	8.0
25	1	1	1	1	1	1
40	0.31	0.28	0.24	0.18	0.2	0.10
60	0.09	0.06	0.055	0.030	0.038	0.011
80	0.033	0.019	0.019	0.007 5	0.011	0.002 3
110	−	−	0.005 9	0.002 0	0.002 6	0.000 42

component moduli thus determined at each temperature are shifted horizontally so that the curves overlap in the terminal regime, to obtain a composite "master" curve for each component for a given blend composition. The values of the horizontal shift factors, $a_{T,i}$, for $T_0 =$ 25 °C for each species are given in Tables 6−8. Uncertainties in the values of $C_i(\phi,T)$ and ϵ affect the magnitude of the component moduli, precluding a meaningful determination of vertical shift.

For the equally entangled blends, where the relaxations of the two components overlap completely, the master curves for the dynamic moduli of both components resemble those of nearly monodisperse homopolymers.[4] This indicates the absence of complications due to differences in the terminal relaxation times of the two components in the blend. The shape and magnitude of the component dynamic moduli are not sensitive to uncertainties of ±10% in the C_i's. Accounting for orientational coupling ($\epsilon = 0.35$) primarily modifies the magnitude of the component moduli (by ∼20%), compared to those estimated without orientational coupling.[4]

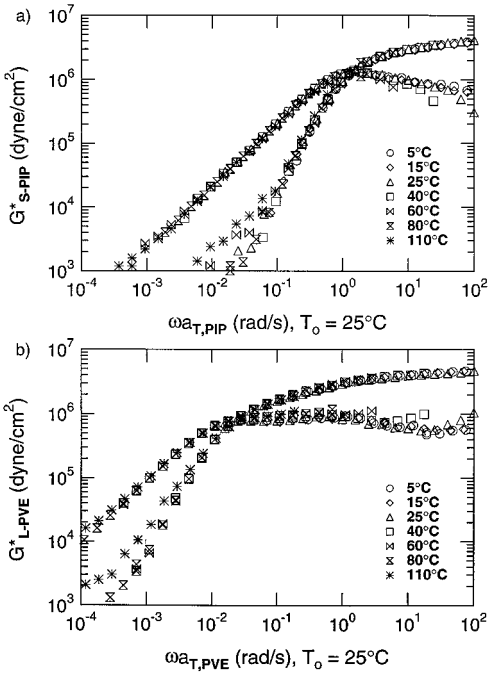

Figure 15. The resulting component moduli for a 50/50 blend of S-PIP/L-PVE. Notice that while the dynamic moduli of the PIP component resemble those of a monodisperse homopolymer, those of PVE exhibit features at higher frequencies which do not superimpose. These are related to the relaxation of the PIP component. See the text for discussion.

Table 8. Shift Factors, $a_{T,i}$, of Each Species in L-PIP/ S-PVE Blends

	blends (PIP/PVE w/w %)					
	75/25		50/50		25/75	
T (°C)	PIP	PVE	PIP	PVE	PIP	PVE
25	1	1	1	1	1	1
40	0.32	0.25	0.25	0.13	0.12	0.11
60	0.087	0.036	0.062	0.021	0.022	0.011
80	0.033	0.011	0.019	0.005 3	0.006	0.002 2
110	0.012	0.003 3	0.006 3	0.001 4	0.001 9	0.000 4
130	0.008	0.001 9	0.003 9	0.000 8	0.001 2	0.000 18

As the difference between the components' relaxation times in the blend increases, the effects of polydispersity become evident.[19−21,31] While the dynamic moduli of the faster relaxing species resemble those of a monodisperse homopolymer, those of the slower relaxing species possess features due to the relaxation of the faster relaxing species. Further, since the temperature dependence of the friction coefficient is different for the two species, the shape of the relaxation spectrum of the long chains changes with temperature (Figures 15 and 16). While time−temperature superposition still holds for the faster relaxing species (and for both species in equally entangled blends, Table 6), it fails for the long chains, since their constraint release relaxation shifts with the short chains and their terminal relaxation shifts with the temperature dependence of the long chains. Therefore, the shift factors of the slower relax-

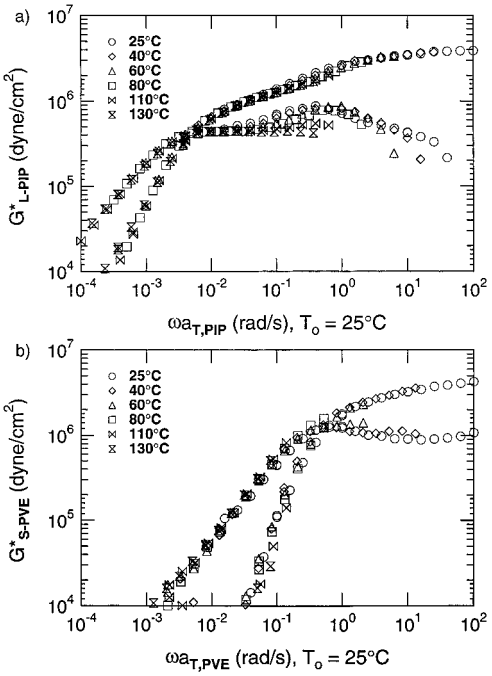

Figure 16. The resulting component moduli for a 50/50 blend of L-PIP/S-PVE. Notice that while the dynamic moduli of the PVE component resemble those of a monodisperse homopolymer, those of PIP exhibit features at higher frequencies which do not superimpose. These are related to the relaxation of the PVE component. See the text for discussion.

ing species are based on superposing their terminal responses (Tables 7 and 8).

Finally, as was previously observed,[4] uncertainties in the values of ϵ and the pure-component stress−optic coefficients, C_i's, have a small effect on the component horizontal shift factors. However, these uncertainties do affect the detailed shape and magnitude of the component moduli (hence, entanglement molecular weights).

4.2. Entanglement Molecular Weight of Each Species. The entanglement molecular weights of each component, $M_{e,i}$, can be determined using

$$M_{e,i}(T,\phi) = \frac{\rho(T,\phi)RT}{G^{\circ}_{N,i}(T,\phi)} \tag{7}$$

where ρ is the melt density,[22] R is the universal gas constant, T is the absolute temperature, and $G^{\circ}_{N,i}$ is the component plateau modulus. To examine changes in the component $M_{e,i}$ with composition it is sufficient to compare relative values (Figure 17).

For the components in the equally entangled blends and the faster relaxing components in the unequally entangled blends, it is straightforward to determine the value of the plateau modulus. Since these component moduli resemble those of nearly monodisperse homopolymers, the maximum in the loss modulus can be used to estimate the plateau modulus as $G^{\circ}_N = qG''(\omega''_{max})$. The value of q varies from 3.56 for polymers with narrow molecular weight distribution[37] to approximately 3.9 for slightly broader distributions.[7,18] Our estimate uses $q = 3.6$. For the slower-relaxing species in the unequally entangled blends, the plateau modulus can be estimated from the value of the storage modulus at the frequency of the minimum in G'' above the high-frequency loss peak, $G^{\circ}_N = G'(\omega''_{min})$.

The entanglement molecular weights of each species do not vary significantly (less than ≈40%) over the range of composition (Figure 17). This is not surprising, since the entanglement molecular weights of the pure components are similar. The error bars reflect a 10% uncertainty in the values of the C_i's, the range of ϵ thus determined and our ability to estimate the component plateau moduli. Given the experimental uncertainty, the data are not adequate to test predictions of the detailed shape of the composition dependence of species' $M_{e,i}$ in miscible blends.

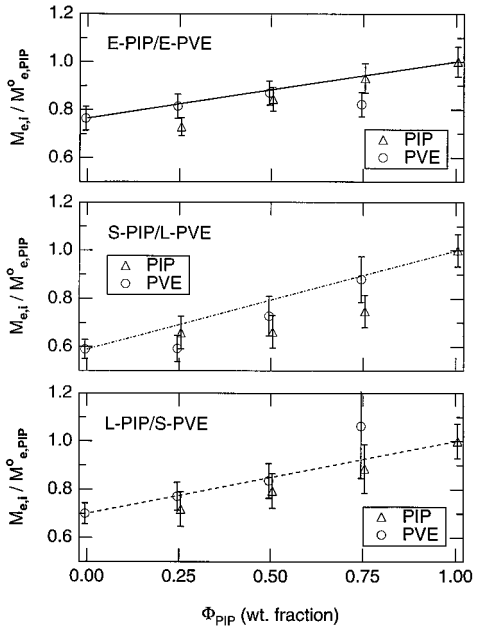

Figure 17. Component entanglement molecular weights in the blends vs weight percent PIP at $T = 25$ °C. **(**a**)** E-PIP/E-PVE, **(**b**)** S-PIP/L-PVE, and **(**c**)** L-PIP/S-PVE. Values are normalized to the value for pure PIP in each case, and horizontally offset for clarity.

4.3. Friction Coefficient of Each Species. The most important information required to understand the complex thermorheological behavior of miscible blends is the effect of composition and temperature on the friction coefficients of the component polymers. This information can be extracted from the rheo-optical results in a way that is insensitive to the particular choice of model used to analyze the data. For all molecular models, the terminal relaxation time of species i takes the form

$$\tau_{d,i} = f\frac{\zeta_{o,i}}{k_B T} \tag{8}$$

where $\zeta_{o,i}$ is the monomeric friction coefficient, and the prefactor f is a model-dependent function of parameters that include the molecular weight of species i and its entanglement molecular weight.[32,39] Since f is essentially independent of temperature and blend ratio (when component molecular weights are close enough to avoid tube-dilation effects), the inferred dependence of $\zeta_{o,i}$ on temperature and composition is the same for all models. Here the effect of blending on the monomeric friction coefficient of each species is inferred by examining the component relaxations within the context of the reptation model.[38,39] In the unequally entangled blends used here, the relaxation times of the slower relaxing component are not affected by tube dilation,[18−21,31] so it is appropriate to relate the terminal relaxation time of both species to their friction coefficient by

$$\tau_{d,i} = \zeta_{o,i}\left(\frac{M_i}{m_{o,i}}\right)\left(\frac{M_i}{M_{e,i}}\right)^2 \frac{a_i^2}{\pi^2 k_B T} \quad (9)$$

where for species i, M_i is the molecular weight of the chain, and $m_{o,i}$ is the monomer molecular weight. The tube diameter, a_i, characterizes the extent of lateral excursions of the i chain among its neighbors, and is related to the radius of gyration, $R_{g,i}$ as

$$a_i^2 = \frac{6R_{g,i}^2 M_{e,i}}{M_i} \quad (10)$$

The temperature dependence of $R_{g,i}$ is neglected since it hardly varies over the experimental range.[17] In PIP/PVE blends, for which $\chi \approx 0$, the $R_{g,i}$ are unaffected by blending. The terminal relaxation time of each component is estimated as $\tau_{d,i}(\phi,T) \simeq 2/\omega_{x,i}$, where $\omega_{x,i}$ is the cross-over frequency for each component i.[4] The friction coefficient of each species at $T = 25$ °C is evaluated using eqs 9 and 10 with the component $M_{e,i}$ determined in the previous section.

Since the shift factors, $a_{T,i}$, represent the scaling of the relaxation dynamics with temperature and the monomeric friction coefficient scales as $\tau_d T$, we determine the temperature-dependent $\zeta_{o,i}$ by scaling the values at $T_o = 25$ °C by $a_{T,i}(T)$ at each temperature. The monomeric friction coefficients of both species decrease with T and with ϕ_{PIP} (Figure 18). The main trends are that the dynamics of the PVE component in all three blend systems depend more on composition and temperature than those of PIP, in agreement with previous studies.[4,18,22] The values of $\zeta_{o,PIP}$ and $\zeta_{o,PVE}$ depend differently on temperature for a given blend composition, consistent with the observed failure of time−temperature superposition. This difference is greatest in blends rich in the high-T_g component (PVE). The temperature dependencies of the component monomeric friction coefficients are independent of molecular weight, as expected for systems with $\chi \lesssim 0$ (*i.e.*, species friction coefficients agree to within a factor of ~2 for all three blend systems).

The curves in Figure 18 correspond to WLF fits to the data based on values from Roovers and Toporowski.[22] For both components in all three sets of blends, there is good agreement between the WLF dependence inferred by Roovers and Toporowski and the present results for $\zeta_{o,i}$. We apply only a vertical shift to $a_{T,i}T$ using their WLF curves for $a_{T,i}$ to yield the best fit to the monomeric friction coefficient data.[4] The values of $C_{1,i}^g$, $C_{2,i}^g$, and $T_{g,i}$ for both components in the pure state and in the blends are given in Table 9. Roovers and Toporowski used values of $C_{1,i}^g = 11.8$ and $C_{2,i}^g = 55$ K, the average values for the pure components, for both components in all the blends. The $T_{g,i}(\phi)$'s for the components in the blends are taken from the average of the values given in Table 6 of their paper.

5. Conclusions

Simultaneous analysis of the shear stress σ_{12} and birefringence n_{12} was used to extract the relaxation spectra of each component in miscible PIP/PVE blends for several combinations of relative component molecular weights. When the species' relaxations in the blend are well-separated, the value of the coupling parameter, ϵ, can be determined. The values $\epsilon_{PIP,PVE} \approx 0.35 \pm 0.04$ and $\epsilon_{PVE,PIP} \approx 0.27 \pm 0.08$ lie within the range established for other systems.[7,18,36] Within experimental uncertainty it appears appropriate to use a single average value of ϵ, independent of temperature and composition. The main trends observed in $M_{e,i}$ and $\zeta_{o,i}$

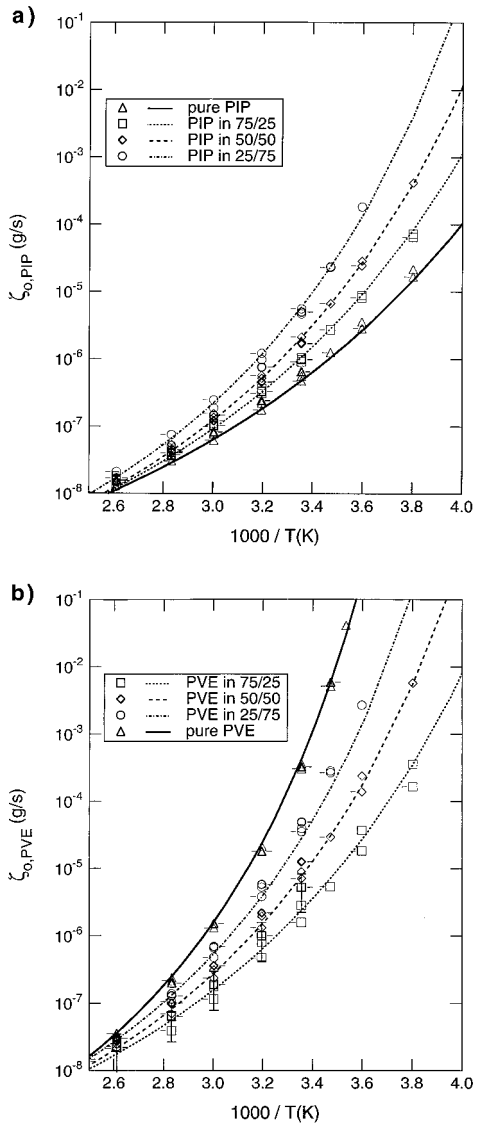

Figure 18. Component monomeric friction coefficients of each species in the blends: (a) PIP and (b) PVE. Symbols for the three families of blends are distinguished by "pips": no pip for E-PIP/E-PVE, left-pip for S-PIP/L-PVE and right-pip for L-PIP/S-PVE. Pure component friction coefficients are shown for reference. Curves correspond to *WLF* fits where $C_{1,i}^g$, $C_{2,i}^g$, and $T_{g,i}$ are taken from Roovers et al. See the text for discussion. Error bars reflect the uncertainties in the C_i's and ϵ, and the corresponding values determined for $M_{e,i}(\phi)$, as well as in $\tau_{d,i}(\phi,T)$, due to uncertainties in the $a_{T,i}$. The uncertainty in $\zeta_{o,i}$ is generally smaller than the size of the symbols. Only for the PVE component in the L-PIP/S-PVE blends are the errors bars larger than the symbols.

Table 9. WLF Paramters from Roovers and Toporowski, Table 6[22]

ϕ_{PIP}	$C_{1,i}^g$	$C_{2,i}^g$ (K)	$T_{g,i}$ (°C)
	PIP		
1	12.0	52.9	−61.0
0.75	11.8	55	−47.0
0.5	11.8	55	−37.5
0.25	11.8	55	−31.0
	PVE		
0.75	11.8	55	−40.0
0.5	11.8	55	−27.5
0.25	11.8	55	−17.5
0.0	11.4	57.5	2.0

are the same as determined previously:[4] (i) blending does not greatly affect the values of $M_{e,i}$ and (ii) it is the species' monomeric friction coefficients that are most sensitive to blending, with those of the high T_g component, PVE, depending more strongly on temperature and composition.

Acknowledgment. We gratefully acknowledge the support of the National Science Foundation Presidential Young Investigator Award (J.A.K.), the National Physical Science Consortium (B.H.A.), the Petroleum Research Fund administered by the American Chemical Society, Chevron, and the Caltech Consortium in Chemistry and Chemical Engineering: E. I. du Pont de Nemours and Company, Inc. and Eastman Kodak Company.

References and Notes

(1) Amram, B.; Bokobza, L.; Sergot, P.; Monnerie, L.; Quesdel, J. P. *Macromolecules* **1990**, *23*, 1212.
(2) Fuller, G. G.; Ylitalo, C. M. *J. Non-Cryst. Solids* **1992**, *131*, 676.
(3) Saito, H.; Miyashita, H.; Inoue, T. *Macromolecules* **1992**, *25*, 1824.
(4) Arendt, B. H.; Kannan, R. M.; Zewail, M.; Kornfield, J. A.; Smith, S. *Rheol. Acta*, **1994**, *33*, 322. Arendt, B. H.; et al. *Proceedings of the ACS, PMSE, Washington, DC*, **1994**, *71*, 471.
(5) Osaki, K.; Takatori, E.; Ueda, M.; Kurata, M.; Kotaka, T.; Ohnuma, H. *Macromolecules* **1989**, *22*, 2457.
(6) Lodge, T. P.; Lodge, A. S. *Rheol. Acta* **1992**, *31*, 32.
(7) Zawada, J. A.; Fuller, G. G.; Colby, R. H.; Fetters, L. J.; Roovers, J. *Macromolecules* **1994**, *27*, 6851.
(8) Bahani, M.; Laupretre, F.; Monnerie, L. *J. Polym. Sci., Polym. Phys. Ed.* **1995**, *33*, 67.
(9) Miller, J. B.; McGrath, K. J.; Roland, C. M.; Trask, C. A.; Garroway, A. N. *Macromolecules* **1990**, *23*, 4543.
(10) Zhao, J.; Chin, Y. H.; Liu, Y.; Jones, A. A.; Inglefield, P. T.; Kambour, R. P.; White, D. M. *Macromolecules* **1995**, *28*, 3881.
(11) Chung, G. C.; Kornfield, J. A.; Smith, S. D. *Macromolecules* **1994**, *27*, 964.
(12) Chung, G. C.; Kornfield, J. A.; Smith, S. D. *Macromolecules* **1994**, *27*, 5729.
(13) Hasagawa, H.; Sakurai, S.; Takenaka, M.; Hashimoto, T.; Han, C. C. *Macromolecules* **1991**, *24*, 1813.
(14) Sakurai, S.; Jinnai, H.; Hasegawa, H.; Hashimoto, T.; Han, C. C. *Macromolecules* **1991**, *24*, 4839.
(15) Roland, C. M. *Macromolecules* **1987**, *20*, 2557.
(16) Roland, C. M. *J. Polym. Sci. Polym. Phys. Ed.* **1988**, *26*, 839.
(17) Tomlin, D. W.; Roland, C. M. *Macromolecules* **1992**, *25*, 2994.
(18) Zawada, J. A.; Fuller, G. G.; Colby, R. H.; Fetters, L. J.; Roovers, J. *Macromolecules* **1994**, *27*, 6861.
(19) Doi, M.; Graessley, W. W.; Helfand, E.; Pearson, D. S. *Macromolecules* **1987**, *20*, 1900.
(20) Rubinstein, M.; Helfand, E.; Pearson, D. S. *Macromolecules* **1987**, *20*, 822.
(21) Struglinski, M. J.; Graessley, W. W. *Macromolecules* **1985**, *18*, 2630.
(22) Roovers, J.; Toporowski, P. M. *Macromolecules* **1992**, *25*, 3454.
(23) Trask, C. A.; Roland, C. M. *Macromolecules* **1989**, *22*, 256.
(24) Carella, J. M.; Graessley, W. W.; Fetters, L. J. *Macromolecules* **1984**, *17*, 2775.
(25) Gotro, J. T.; Graessley, W. W. *Macromolecules* **1984**, *17*, 2767.
(26) Kannan, R. M.; Kornfield, J. A. *Macromolecules* **1994**, *27*, 1177.
(27) Kannan, R. M.; Kornfield, J. A. *Journal of Rheology* **1994**, *38*, 1127.
(28) Janeschitz-Kriegl, H. *Polymer Melt Rheology and Flow Birefringence*; Springer-Verlag: Berlin, 1983.
(29) Ferry, J. D. *Viscoelastic Properties of Polymers*; Wiley: New York, 1980.
(30) Read, B. E. *Polymer* **1962**, *3*, 143.
(31) Kornfield, J. A.; Fuller, G. G.; Pearson, D. S. *Macromolecules* **1991**, *24*, 5429.
(32) Larson, R. G. *Constitutive Equations for Polymer Melts and Solutions*; Butterworths: Boston, 1988.
(33) Osaki, K.; Takatori, E.; Kurata, M.; Ohnuma, H.; Kotaka, T. *Polymer* **1986**, *18*, 947.
(34) Baljon, A. R. C.; Grest, G. S.; Witten, T. A. *Macromolecules* **1995**, *28*, 1835.
(35) Doi, M.; Pearson, D. S.; Kornfield, J. A.; Fuller, G. G. *Macromolecules* **1989**, *22*, 1488.
(36) Ylitalo, C. M.; Zawada, J. A.; Fuller, G. G.; Abetz, V.; Stadler, R. *Polymer* **1992**, *33*, 2949.
(37) Raju, R. V.; Menezes, E. V.; Martin, G.; Graessley, W. W. *Macromolecules* **1981**, *14*, 1668.
(38) deGennes, P. G. *J. Chem. Phys.* **1971**, *55*, 572.
(39) Doi, M.; Edwards, S. F. *The Theory of Polymer Dynamics*; Oxford University Press: Oxford, 1986.
(40) Alegria, A.; Colmenero, J.; Ngai, K. L.; Roland, C. M. *Macromolecules* **1994**, *27*, 4486.

MA960901L